EVALUATION OF AN UNMANNED AERIAL VEHICLE (UAV) FOR MEASURING AND MONITORING NATURAL DISASTER RISK AREAS

M. L. L. Reiss[1*], T. S. G. Mendes[2], F. F. Pereira[4], M. R. M. de Andrade[3], R. M. Mendes[3], S. J. C. Simões[2], R. de Lara[5], S. F. de Souza[5]

[1]LAFOTO – Laboratory of Photogrammetry Research, Department of Geodesy, Institute of Geoscience, UFRGS – Federal University of Rio Grande do Sul, Brazil – (mario.reiss, lafoto)@ufrgs.br
[2]Department of Environmental Engineering, Institute of Science and Technology – ICT, São Paulo State University – Unesp, São José dos Campos, São Paulo, Brazil – (tatiana.mendes, silvio.simoes)@unesp.br
[3]National Center for Monitoring and Early Warning of Natural Disasters - CEMADEN, São José dos Campos, São Paulo, Brazil – marcio.andrade@cemaden.gov.br
[4]Graduate Program in Natural Disasters, UNESP/CEMADEN, São José dos Campos, São Paulo, Brazil – felicia.franca@unesp.br
[5]LAGEO – Laboratory of Geodesy, Department of Geodesy, Institute of Geoscience, UFRGS – Federal University of Rio Grande do Sul, Brazil – (rooseveltdelara, sergio.florencio)@ufrgs.br

Commission II, WG II/10

KEY WORDS: Photogrammetry with UAV-RPAS-PPK, No Need for Control Points, Topographic Mapping, Natural Disasters, Risk Areas, Monitoring of Environmental Risks.

ABSTRACT:

This work presents an evaluation of a small UAV-RPAS-PPK to be used in the generation of digital surface models (DSM), without the need for control points, having as main application the monitoring of disaster risk areas (landslide and flooding). The areas to be measured are difficult to access, which prevents or makes access to the land difficult. In this evaluation, a study area of approximately 13 km² was flown over, an average pixel of 11.6 cm and a total of 417 photos. The equipment used to acquire the images was a SenseFly eBee X, equipped with GNSS PPK for Direct Georeferencing (DG) and a camera model S.O.D.A. In all, 42 ground checkpoints were measured using a dual-frequency GNSS receiver. For both the measurement of the checkpoints and for the Direct Georeferencing (DG) base of the Unmanned Aerial Vehicles (UAV), a relative processing was performed, using the Brazilian Network for Continuous Monitoring (RBMC) as a reference. With this evaluation, it was possible to achieve a result (RMSE) for phototriangulation better than 1.2 pixels for horizontal and 1.5 pixels for vertical, without the need to measure any control points on the ground.

1. INTRODUCTION

Due to climate change, one of the biggest problems today is the occurrence of extreme weather events such as storms, floods, and landslides. These, in turn, combined with inadequate and disorderly urban occupation, cause great economic impacts and risks to people's lives. Hydrogeological impacts due to floods and landslides are among the most significant disasters in the world (Marta et al., 2020).

For the mapping and monitoring of disaster risk areas, there is a need for an updated database with its known qualities, in a context of rapid changes due to human activities and occupation and the climate events to which some areas are susceptible. It is also important to consider that in many risk areas, it is difficult or even impossible to access the study site for on-site mapping measurements, and there may be a risk to the people involved in this activity.

Unmanned Aerial Vehicles (UAV) data have been widely used for high resolution mapping and are presented as a low-cost alternative to photogrammetric acquisitions involving conventional platforms and cameras. In this sense, three-dimensional geospatial data has the potential to provide essential information for decision-making (Fazeli et al., 2016) and to support disaster mitigation, prevention, and response strategies.

With the popularization of the UAV technology, several applications are found in the literature involving the issue of disasters related to landslides and floods (or hydrogeological disasters). As examples, analysis of road surface deformation caused by a landslide (Cardenal et al., 2019), identification of flooded areas (Giordan et al., 2017), and forensic geomorphological analysis to characterize a landslide-triggered debris flow (Cabral et al., 2021). However, there are few works that present the cartographic quality of the products generated from UAV data. Chiarando et al. (2019) state that the geospatial component in UAV data shall be properly considered through fast but rigorous photogrammetric processing aimed at generating 3D models and orthoimages of the surveyed areas.

The National Center for Monitoring and Early Warning of Natural Disasters (CEMADEN) and partner institutions, such as the Federal University of Rio Grande do Sul (UFRGS) and the São Paulo State University (UNESP), through the REMADEM/REDEGEO Project, have been exploring the use of UAV data to support studies in hydrogeological risk areas. The CAPES Pro-Alertas project, developed by the institutions Pontifical Catholic University of Rio Grande do Sul (PUC-RS) and UFRGS from 2014 to 2019, with the objective of integrating autonomous vehicles and sensor networks, also had its focus directed to acquisition remote data for the prevention and mitigation of natural disasters, with the development of a

* Corresponding author

methodology for monitoring risk areas using Digital Surface Models (DSMs) produced using UAV technology.

In the development of the work, two surveying were carried out. The first was a risk area in the City of Blumenau, in the State of Santa Catarina, using a SenseFly eBee Classic UAV. According to the characteristics of this equipment, there was necessary to acquire control points on the ground, which made the work very difficult due to the impossibility of accessing various areas of the terrain (Reiss et al., 2018). The second surveying, which is the main discussion topic of this work, was carried out in the City of Santos, State of São Paulo, with a SenseFly eBee X UAV. Despite the statement of the manufacturer that there would be no need to acquire control points on the ground, up to a horizontal accuracy varying between 1 to 3 times the Ground Sampled Distance (GSD) (Roze et al, 2014), it is necessary to verify if in practice this statement and that quality of the products to be generated is true. Thus, where Ground Control Points (GCP) acquisition is impeded by site access difficulties or hazardous circumstances, Direct Georeferencing (DG) can be used (Ekaso et al., 2020).

Based on this statement, the hypothesis to be verified is whether it is possible to obtain a positioning quality as recommended by the manufacturer for without the use of ground control points. In this sense, this work aims to evaluate the quality of the 3D point cloud generated from data obtained with the SenseFly eBee X considering different photogrammetric processing configurations and the possibility of not needing the use of GCP.

2. MATERIALS AND METHODOLOGY

2.1 Platform

The platform used in this work is the previously mentioned equipment, the SenseFly eBee X, with the ability to perform DG through an integrated dual-frequency GNSS, which allows the correction of the position of the images during or after the acquisition. The sensor used was a S.O.D.A. The main sensor characteristics are presented in Table 1.

Camera	S.O.D.A.
Nominal focal length	10.6 mm
Resolution	5472x3648 px / 20 megapixels
Pixel size	2.34 µm

Table 1. Main sensor characteristics.

The equipment operating software is named eMotion 3, which allows both the planning and execution of photogrammetric coverage. Several functionalities are available, allowing different modes of equipment operation and coverage configurations of the area of interest. It is intuitive to use, favoring operation by lay users, with a minimum of training.

2.2 Case Study

The area selected for the case study is a place of real interest for CEMADEN. It is in the city of Santos, in the State of São Paulo, Brazil, as shown in Figure 1.

The main area of interest, represented in Figure 1 by the central polygon in blue, contains approximately 2.3 km². This area comprises the Morros de Santos, an area of high risk of landslides, especially in extreme rainfall events. The area of interest (Figure 1) has regions that are difficult to access and some of them dominated by criminal factions, which makes it difficult or even impossible to measure control and check points. As an alternative to this problem, a larger area, represented in Figure 1 by the pink polygon, was defined as an area of interest for acquiring the photos. The idea was to measure checkpoints around the area of interest, not within it, to avoid the risk area, so we ended up surveying a larger area.

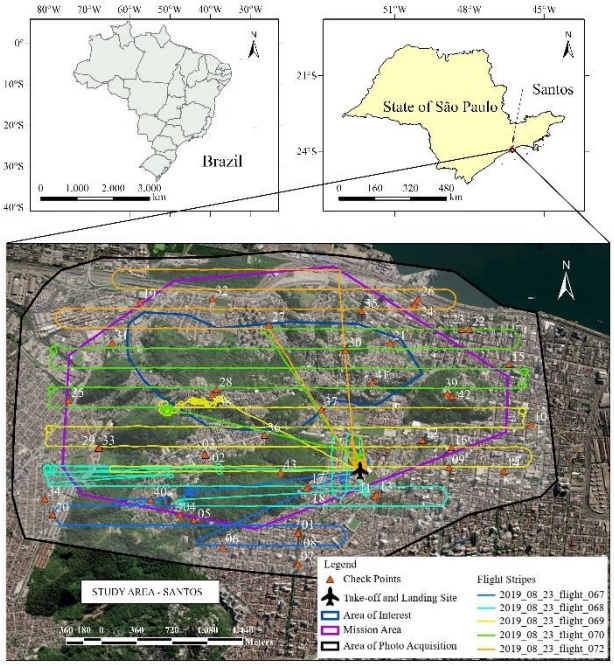

Figure 1. Case Study: City of Santos in State of São Paulo, Brazil.

The GSD planned for the acquisition of photographs was 12 cm, but in view of the variation in relief in the study area, the average GSD performed was 11.6 cm. With this size of GSD the flight height was approximately 530 m. Being a risk area also because of crime, this height of flight made it possible for the UAV to perform a flight without being noticed by the local residents and/or by someone who could shoot it down. The lateral and longitudinal overlaps were defined as 60% and 75%, respectively. Table 2 summarizes the main parameters established for the flight plan.

GSD	12 cm/px
Lateral overlap	60%
Longitudinal overlap	75%
Flight altitude	530 m
Between photos	109 m
Flight line spacing	263 m

Table 2. Summary of flight plan data.

The flight plan parameters were entered into the eBee X operating software, the eMotion 3 software and the photo acquisition were performed (Figure 2). The result of the acquisition, which was carried out on August 23, 2019, generated a set of 417 photographs, on 5 flights in a total of 15 flight tracks.

A base station was measured at an arbitrary location, close to the landing and take-off point, for the Post-Processing Kinematic (PPK) positioning process of the acquired photos.

As this is an evaluation work, an effort was made, despite the difficulties mentioned, to measure checkpoints. Of the 43 points measured on the ground, 42 remained after the elimination of 1, as it was identified as containing a gross error. The survey of the checkpoints was carried out in 4 days, between the 13th to the 15th and on the 25th of November 2021. This time lapse of 2 years and three months between the acquisition of the photographs and the measurement of the checkpoints was due to logistical difficulties caused by the worldwide pandemic of covid-19.

To obtain the best possible quality for phototriangulation adjustment, it was considered to distribute the points, as much as possible, regularly spaced between them and covering the entire area of interest. Another important feature was that the points were photoidentifiable, as in corners for example.

Another arbitrary basis was established for the measurement of checkpoints. The measurement of the coordinates of the bases, both for the flight and for the checkpoints, was performed by tracking GNSS data, using dual-frequency Leica Viva GS-15 RTK GNSS receivers.

Figure 2. Flight plan simulation run by eMotion: eBee X operating software.

2.3 GNSS Processing

The processing of the DG coordinates of the photos acquired with the UAV used is like what was performed for the measurement of checkpoints. In both cases, it is necessary to establish a reference base for the relative processing of GNSS coordinates (Figure 3).

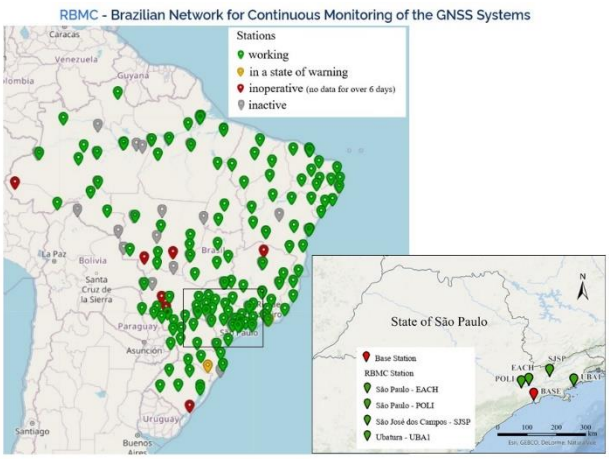

Figure 3 – Structure of the Brazilian GNSS Network (RBMC) used for GNSS base coordinates calculated for the relative post-processing of image and checkpoint coordinates.

The difference is that for the coordinates of the photos the positioning is the Kinematic Relative and in the case of the checkpoints it is the Static Relative (Cledat et al., 2020). In both cases, there was no need to materialize the base coordinates on the ground. They were calculated for the antenna phase center. The GNSS receiver was installed close to the survey region and the processing was carried out using coordinate transport through the stations of the Brazilian Network for Continuous Monitoring (RBMC) of the GNSS System (Figure 3), available in the national territory and whose data can be accessed by the website of the Brazilian Institute of Geography and Statistics (IBGE, 2022).

The RBMC reference stations that were used to calculate the base for the DG, named DG_BASE, are: POLI, EACH and UBA1 (IBGE, 2022). Table 3 shows the coordinates that were adjusted:

Zone 23 K			
	UTM (m)	Geog. (gms)	RMS (m)
Est/Long	363763.157	46°20'19.69103"W	0.008
North/Lat	7351170.639	23°56'43.49488"S	0.008
h (m)	2.429		0.020
Hz			0.011

Table 3. Adjusted base of DG photos

Once this base was calculated, the coordinates of the Perspective Centers (PC) of each of the 417 photos that were acquired in the photogrammetric survey with SenseFly eBee X were calculated using PPK, through the eMotion software in its PostFlight module. As it is a large volume of data, these data will not be shown here.

BASE_21-10-13 (m) – Zone 23 K			
	UTM (m)	Geog. (gms)	RMS (m)
Est/Long	362661.681	46°20'58.41910"W	0.008
North/Lat	7351853.099	23°56'20.96886"S	0.008
h (m)	173.278		0.023
Hz			0.011
BASE_21-10-14 (m) – Zone 23 K			
	UTM (m)	Geog. (gms)	RMS (m)
Est/Long	362661.680	46°20'58.41915"W	0.008
North/Lat	7351853.098	23°56'20.96889"S	0.008
h (m)	173.329		0.020
Hz			0.010
BASE_21-10-15 (m) – Zone 23 K			
	UTM (m)	Geog. (gms)	RMS (m)
Est/Long	362661.679	46°20'58.41917"W	0.007
North/Lat	7351853.087	23°56'20.96924"S	0.007
h (m)	173.318		0.023
Hz			0.010
BASE_21-10-25 (m) – Zone 23 K			
	UTM (m)	Geog. (gms)	RMS (m)
Est/Long	362661.671	46°20'58.41945"W	0.007
North/Lat	7351853.097	23°56'20.96892"S	0.007
h (m)	173.318		0.023
Hz			0.010

Table 4. Adjusted (computed) Bases for checkpoints processing.

In a similar way, it was done with the coordinates of the bases determined for the survey of the checkpoints. This survey took place over 4 days (October 14 to 15 and 25, 2021), taking measurements on 4 different bases, one for each day. Each processing of the bases was then calculated independently of each other, with the respective processing of the irradiations of the coordinates of the checkpoints, surveyed on the same day, synchronously with their base. The adjusted values of the base coordinates for the checkpoint calculation are presented in Table 3. Following, in Table 4 are the checkpoint coordinates.

id	UTM (m)			STD (m)		
	E	N	h	sE	sN	sh
01_g	363233.160	7350467.944	-1.424	0.010	0.009	0.026
02_g	362365.659	7351216.812	74.591	0.012	0.011	0.034
03_g	362356.071	7351229.567	74.837	0.014	0.012	0.035
04_g	362131.071	7350620.862	85.646	0.009	0.009	0.024
05_g	362262.548	7350569.963	107.957	0.010	0.009	0.028
06_g	362530.896	7350308.521	-1.321	0.009	0.010	0.027
07_g	363234.015	7350143.140	-1.530	0.009	0.010	0.026
08_g	363231.779	7350452.648	-1.305	0.011	0.011	0.033
09_g	364632.459	7351118.974	-1.077	0.015	0.025	0.046
10_g	365393.358	7351554.921	-2.442	0.012	0.010	0.032
11_g	363941.703	7350825.400	-1.418	0.011	0.010	0.023
12_g	364384.454	7351384.633	-2.090	0.016	0.013	0.037
13_g	363961.474	7350844.081	-1.420	0.014	0.011	0.044
14_g	365144.119	7351085.692	-1.637	0.011	0.013	0.035
15_g	365181.659	7352150.282	-0.870	0.008	0.008	0.023
16_g	364652.881	7351317.175	-1.200	0.014	0.012	0.034
17_g	363322.087	7350919.739	0.930	0.008	0.008	0.022
18_g	363308.859	7350898.018	1.650	0.008	0.007	0.021
19_g	361737.343	7352740.932	-2.153	0.014	0.014	0.040
20_g	360945.654	7350609.986	-2.523	0.012	0.013	0.049
21_g	364074.235	7352351.258	17.099	0.015	0.019	0.048
22_g	364808.908	7352496.838	-0.603	0.014	0.023	0.055
23_g	364741.446	7352494.099	0.395	0.018	0.018	0.069
24_g	364294.626	7352737.619	-0.878	0.019	0.015	0.058
25_g	361080.158	7351751.515	-3.360	0.009	0.010	0.028
26_g	364330.862	7352791.783	-1.328	0.010	0.010	0.031
27_g	362943.440	7352522.690	-2.638	0.010	0.010	0.030
28_g	362457.313	7351870.748	183.147	0.009	0.009	0.029
29_g	361362.107	7351277.040	0.486	0.011	0.009	0.030
30_g	363658.409	7352277.550	150.912	0.009	0.009	0.030
31_g	361483.787	7352327.739	-0.662	0.011	0.013	0.031
32_g	362414.924	7352779.107	-2.557	0.011	0.010	0.029
33_g	361370.945	7351278.787	0.680	0.016	0.010	0.039
34_g	360868.382	7350769.817	-2.563	0.008	0.008	0.027
35_g	363805.466	7352667.321	1.825	0.011	0.011	0.032
36_g	362911.993	7351423.148	77.865	0.012	0.011	0.032
37_g	363440.118	7351683.442	4.542	0.015	0.014	0.044
38_g	362419.893	7351824.320	177.086	0.008	0.008	0.026
40_g	361855.950	7350770.270	70.760	0.008	0.008	0.025
41_g	363911.619	7351959.681	81.088	0.009	0.010	0.033
42_g	364653.907	7351824.056	153.411	0.017	0.014	0.044
43_g	363066.666	7351053.521	101.641	0.009	0.009	0.027

Table 5 – Checkpoints in UTM (Zone 23 K) coordinate, in meters.

2.4 Photogrammetric Processing

The photogrammetric processing was performed in this work exclusively using the software Agisoft Metashape Professional Educational Edition, version 1.8.1. The first procedure performed was to insert the photos and assign to them the positions of the PCs calculated by the PPK processing performed in eMotion PostFlight and made available in a file. In the sequence, an automatic alignment (phototriangulation) of the photograph was performed, considering only the PCs as a control point. Bearing this in mind, a low-quality orthophoto was produced to allow locating photoidentifiable points, possible candidates for checkpoints to be located and measured on the ground. This occurred the day after the photo acquisition was carried out as soon as the processing of the base coordinates for the DG was ready. 43 points were then selected, of which 1 had gross errors and was eliminated. Left 42 points that were considered as tie points in a new phototriangulation process. This was performed, now considering better quality condition for the image processing parameters.

2.5 Experiment conditions

To define a better quality for the accomplishment of this work, some experimental combinations involving setup forms of photogrammetric processing was made:

Setup 1:

1. Consider the coordinates of the GNSS base as a fixed (absolute injunction) in the DG's post-processing (Figure 4 (a)).
2. Consider the coordinates of the GNSS base as a relative variable (relative injunction) in the post-processing of the DG (Figure 4 (b)).

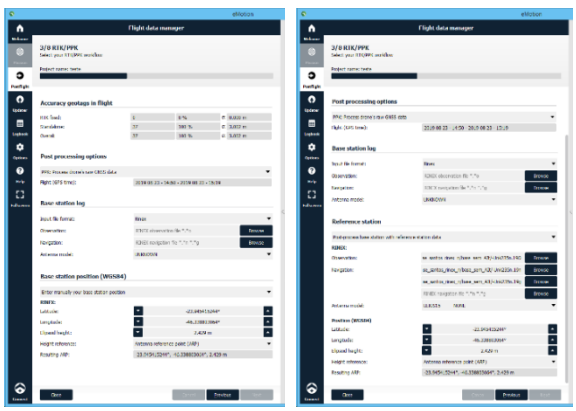

(a) (b)

Figure 4 – DG post-processing considering the base coordinates as: (a) fixed; (b) variables and recalculated by the Rinex file as processing information.

Setup 2:

1. Perform a new alignment of the photogrammetric block (phototriangulation/optimize cameras) without automatic detection of new tie points after manually measuring the checkpoints in the photos (Figure 5).
2. Perform a new alignment of the photogrammetric block (phototriangulation) but detecting new automatic tie points (Figure 5).

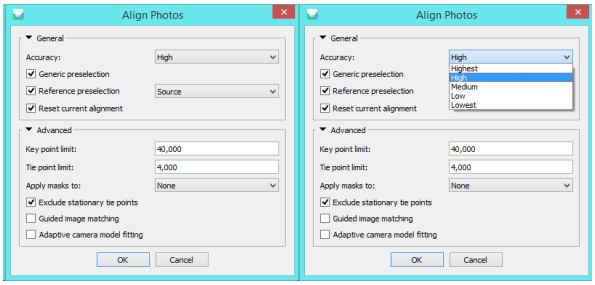

Figure 5 – Selection of the accuracy (number of points) that will be automatically detected as tie points for the alignment process (image matching and phototriangulation).

Setup 3:

1. Use a photogrammetric block in which its accuracy was defined as **high** in its alignment (Figure 5).
2. Use a photogrammetric block in which its accuracy was defined as **low** in its alignment (Figure 5).

In 1 or 2, it was noticed that there was a difference in the quality of the phototriangulation result when it was used to fix the base coordinates for the DG or inform the base values and inform the Rinex file for the eMotion PostFlight module to recalculate the value of the base as a relative injunction.

Another change noticed in the results was after measuring the checkpoints in the photos (which work as tie points in the phototriangulation) that there was a change in the result if the automatic process of tie points detection by correspondence and a new phototriangulation were performed again.

Finally, it is known that the number of points detected for the image matching process interferes with the phototriangulation result. In this situation, it was chosen to test the accuracy of a High or Low point, seeking a better cost-effective processing ratio.

2.6 Statistical metrics

The verification of the quality of phototriangulation occurred by comparing the coordinates of the checkpoints measured in the photos (*m*) and calculated for the terrain by phototriangulation and the coordinates of their equivalent measured on the ground itself by means of GNSS (*g*). For this, the discrepancies between the points were then calculated (1):

$$d_{x_i} = P_{mi} - P_{g_i} \,, \tag{1}$$

where: d_x are the discrepancies;

P_m are the measurements taken from the images, calculated for the ground by triangulation;

P_g are the measurements taken directly on the ground by GNSS;

And the following statistics (2) to (6):

$$\mu_{d_x} = \frac{1}{n}\sum_{i=1}^{n} d_{xi} \,, \tag{2}$$

$$\sigma_{d_x} = \sqrt{\frac{1}{n-1}\sum_{i=1}^{n}\left(d_{xi} - \mu\right)^2} \,, \tag{3}$$

$$RMSE_{d_x} = \sqrt{\frac{1}{n}\sum_{i=1}^{n}\left(d_{xi}\right)^2} \,, \tag{4}$$

$$t_x = \frac{\mu_{d_x}}{\sigma_{d_x}} \cdot \sqrt{n} \,, \tag{5}$$

$$\chi^2{}_x = \left(n-1\right) \cdot \frac{{\sigma_{d_x}}^2}{\sigma_e^2} \,, \tag{6}$$

where: μ_{d_x} is the mean of the discrepancies;

σ_{d_x} is the standard deviation of the sample;

n is the sample size;

$RMSE_{d_x}$ is the root-mean-square error;

t_x is the t-Student statistic for sample;

$\chi^2{}_x$ is the chi-square statistic for sample;

σ_e is the standard deviation expected for the sample.

Considering

$$t_{(n-1,\alpha/2)} \tag{7}$$

and

$$\chi^2_{(n-1,\alpha)} \tag{8}$$

being the theoretical t-Student (7) and chi-square (8) functions, respectively, for a significance level α, is possible calculate (9):

$$\sigma_e^2 = \left(n-1\right) \cdot \frac{{\sigma_{d_x}}^2}{\chi^2_{(n-1,\alpha)}} \,. \tag{9}$$

3. RESULTS AND ANALYSIS

3.1 Results

To analyze whether it is possible to eliminate the need for control points, an analysis of the discrepancies between the values from the phototriangulation and those measured on the ground was performed. For this, it was necessary to define some input parameters for the statistical analysis. These parameters are shown in Table 6.

Sample size		42
Unit of Measure		(m)
Pixel Size	(cm)	11.6
Significance level	(%)	5.00
Probability	(%)	95.00
t-Student (theoretical)		2.020
Expected quality	(cm)	15.50
Expected quality	(m)	0.155
Chi-square (theoretical)		56.942

Table 6 –Input data for statistical analysis

From these input data, the analysis data presented in Table 7 were calculated. After the phototriangulation analysis was performed, an orthophoto of the photogrammetric block was produced, as shown in Figure 6.

Nº of Experiment	Setups	Coord.	BIAS (m)	BIAS (pixel)	STD (m)	STD (pixel)	RMSE (m)	RMSE (pixel)	t-Student test (sample)	Chi-square test (sample)	Accuracy (m)	Accuracy (pixel)
1	Setup1: 2	E	0.041	0.352	0.126	1.088	0.131	1.131	**2.099**	**27.189**	0.107	0.92
	Setup2: 1	N	-0.015	-0.130	0.139	1.197	0.138	1.190	**0.704**	**32.893**	0.118	1.02
	Setup3: 1	h	-0.059	-0.504	0.183	1.580	0.190	1.640	**2.070**	**57.296**	0.155	1.34
2	Setup1: 2	E	0.102	0.881	0.185	1.596	0.210	1.806	**3.577**	**58.485**	0.157	1.35
	Setup2: 1	N	-0.043	-0.372	0.169	1.455	0.172	1.485	**1.658**	**48.626**	0.143	1.23
	Setup3: 1	h	-0.143	-1.233	0.272	2.346	0.190	1.640	**3.406**	**126.353**	0.231	1.99
3	Setup1: 2	E	0.066	0.567	0.127	1.098	0.142	1.224	**3.348**	**27.681**	0.108	0.93
	Setup2: 2	N	-0.033	-0.288	0.135	1.165	0.138	1.186	**1.603**	**31.161**	0.115	0.99
	Setup3: 1	h	-0.049	-0.421	0.197	1.699	0.190	1.640	**1.605**	**66.255**	0.167	1.44
4	Setup1: 1	E	0.040	0.346	0.126	1.087	0.131	1.129	**2.061**	**27.153**	0.107	0.92
	Setup2: 1	N	-0.016	-0.135	0.139	1.194	0.138	1.188	**0.730**	**32.759**	0.118	1.01
	Setup3: 1	h	0.146	1.258	0.183	1.580	0.190	1.640	**5.162**	**57.312**	0.156	1.34
5	Setup1: 1	E	0.102	0.879	0.187	1.616	0.211	1.823	**3.524**	**59.976**	0.159	1.37
	Setup2: 2	N	-0.047	-0.406	0.171	1.476	0.176	1.514	**1.781**	**50.043**	0.145	1.25
	Setup3: 2	h	0.056	0.482	0.275	2.375	0.190	1.640	**1.315**	**129.497**	0.234	2.02
6	Setup1: 1	E	0.064	0.555	0.128	1.101	0.142	1.221	**3.267**	**27.824**	0.108	0.93
	Setup2: 2	N	-0.033	-0.286	0.136	1.174	0.139	1.194	**1.579**	**31.624**	0.116	1.00
	Setup3: 1	h	0.153	1.315	0.198	1.707	0.190	1.640	**4.990**	**66.950**	0.168	1.45
7	Setup1: 2	E	0.023	0.202	0.124	1.072	0.125	1.078	**1.224**	**26.387**	0.106	0.91
	Setup2: 1	N	-0.011	-0.098	0.130	1.125	0.129	1.115	**0.565**	**29.043**	0.111	0.95
	Setup3: 1	h	-0.060	-0.519	0.165	1.423	0.174	1.499	**2.365**	**46.530**	0.140	1.21
8	Setup1: 2	E	0.020	0.174	0.128	1.100	0.128	1.100	**1.028**	**27.761**	0.108	0.93
	Setup2: 2	N	-0.022	-0.193	0.131	1.126	0.131	1.129	**1.110**	**29.089**	0.111	0.96
	Setup3: 1	h	-0.049	-0.422	0.163	1.408	0.169	1.453	**1.943**	**45.498**	0.139	1.19

Table 7 – Result for statistical analysis using different setups of photogrammetric processing

Figure 6 – Printing of the orthophoto generated for the study area.

3.2 Analysis

In all, 8 experiments were carried out with processing parameters varying according to the description contained in Section 2.5. and the indication in the second column of Table 7. The objective was not to perform and present all possible combinations, as this would be impossible, but to present some variations that were shown to have a more significant influence on the results for the output coordinates of the 42 measured checkpoints. But regardless of any of the setups of the experiments we did, the largest RMSE was less than 1.9 in pixel, which was in experiment 5 in the East coordinate.

The best result achieved was experiment 8, having passed the trend test for all coordinate components, since

$$t_x \leq t_{(n-1,\alpha/2)}, \quad (10)$$

it is true.

In the accuracy test, experiment 8 was also the best result, being

$$\chi^2{}_x \leq \chi^2{}_{(n-1,\alpha)}, \quad (11)$$

also true.

In experiment 8 still time a horizontal RMSE less than 1.12 pixels and vertical better than 1.5 pixels.

4. CONCLUSIONS

The results presented in this case study allowed us to verify that the DG applied in data acquired using the SenseFly eBee X can generate products, as a dense cloud point that represents de DSM, with high quality without the need to measure any GCP.

Different configurations for triangulation processing were tested and the best result was achieved using configuration 8, which considers the following conditions: the coordinates of the GNSS base as a relative variable (relative injunction) in the post-processing of the DG; a new alignment of the photogrammetric block (phototriangulation) but detecting new automatic tie points; and using a photogrammetric block in which its accuracy was defined as high in its alignment.

This result was achieved considering the kinematic relative positioning for the CP correction of the photos and the relative static positioning for the coordinates of the checkpoints.

Some other settings for the photogrammetric process will be studied and applied to find ways to improve the results, such as exploring ways to improve the camera calibration consideration. This has not been aborded in this study.

Another subject that can be addressed in future works is the influence of connection points manually measured by a human operator on the final quality of the generated photogrammetric products.

We will now use the photogrammetric products that can be generated for mapping the study area to create a quality DSM and DEM that can be used in flood and landslide simulations.

ACKNOWLEDGEMENTS

The team thanks: to FINEP (REMADEN/REDEGEO Project - Invitation Letter MCTI/FINEP/FNDCT 01/2016) for the financial support; to IPHAN-RS through the Cooperation Term 01/2013 UFRGS/IPHAN-RS; to CAPES by funding of the Pro-Alerts project (88887.091734/2014-01); and to the REUNI project of the Federal Government, which provided the acquisition of part of the equipment used in the work; to UFRGS By Equipment and physical space Transferred to accomplish this work.

REFERENCES

Cabral, V.C., Reis, F.A.G.V., D'Affonseca, F.M. et al., 2021. Characterization of a landslide-triggered debris flow at a rainforest-covered mountain region in Brazil. Nat Hazards 108, 3021–3043. https://doi.org/10.1007/s11069-021-04811-9

Cardenal, J., Fernández, T., Pérez-García, J. L., Gómez-López, J. M., 2019. Measurement of Road Surface Deformation Using Images Captured from UAVs. Remote Sens. 11(12), 1507. https://doi.org/10.3390/rs11121507

Chiabrando, F., Giulio Tonolo, F., Lingua, A., 2019. UAV Direct Georeferencing approach in an Emergency Mapping Context, The 2016 Central Italy Earthquake Case Study. Int. Arch. Photogramm. Remote Sens. Spatial Inf. Sci., XLII-2/W13, 247–253. https://doi.org/10.5194/isprs-archives-XLII-2-W13-247-2019

Cledat, E., Jospin, L.V., Cucci, D.A., Skaloud, J., 2020. Mapping quality prediction for RTK/PPK-equipped micro-drones operating in complex natural environment. ISPRS Journal of Photogrammetry and Remote Sensing, 167, 24-38. https://doi.org/10.1016/j.isprsjprs.2020.05.015.

Ekaso, D., Nex, F., Kerle, N., 2020. Accuracy assessment of real-time kinematics (RTK) measurements on unmanned aerial vehicles (UAV) for direct geo-referencing, Geo-spatial Information Science, 23(2), 165-181. 10.1080/10095020.2019.1710437

Fazeli, H., Samadzadegan, F., Dadrass Javan, F., 2016. Evaluating the Potential of RTK-UAV for automatic Point Cloud Generation in 3D Rapid Mapping. ISPRS - International Archives of the Photogrammetry, Remote Sensing and Spatial Information Sciences. XLI-B6. 221-226. 10.5194/isprsarchives-XLI-B6-221-2016.

Giordan, D., Hayakawa, Y., Nex, F., Remondino, F., Tarolli, P., 2018. Review article: the use of remotely piloted aircraft systems (RPASs) for natural hazards monitoring and management. Nat. Hazards Earth Syst. Sci. 18, 1079–1096. https://doi.org/10.5194/nhess-18-1079-2018

Giordan, D., Notti, D., Villa, A., Zucca, F., Calò, F., Pepe, A.,Dutto, F., Pari, P., Baldo, M., Allasia, P., 2017. Low cost, multiscale and multi-sensor application for flooded areas mapping. Nat. Hazards Earth Syst. Sci. Discuss., https://doi.org/10.5194/nhess- 2017-420, in review, 2017.

IBGE. 2022. Instituto Brasileiro de Geografia e Estatística, Available online: <https://www.ibge.gov.br/geociencias/informacoes-sobre-posicionamento-geodesico/rede-geodesica/16258-re de-brasileira-de-monitoramento-continuo-dos-sistemas-gnss-rb mc.html?=&t=dados-diarios-e-situacao-operacional>. Accessed on 02 Apr 2022.

Marta, E., Guglielmo, R., Giuliana, B., Alessandra, B., Veronica, V., Paola, M., 2020. Past and future hydrogeological risk assessment under climate change conditions over urban settlements and infrastructure systems: the case of a sub-regional area of Piedmont, Italy. Nat Hazards 102, 275–305. https://doi.org/10.1007/s11069-020-03925-w

Reiss, M. L. L., Mendes, T. S. G., Andrade, M. R. M., Mendes, R. M., 2018. Mapeamento fotogramétrico com uso de VANT para a Avaliação de Áreas de Risco Geológico na Cidade de Blumenau-SC. VII Simpósio Brasileiro De Ciências Geodésicas e Tecnologias da Geoinformação. Recife, PE, 08-09 nov.

Roze, A., Zufferey, J.-C., Beyeler, A., McClellan, A. eBee RTK Accuracy Assessment. White Paper Sense Fly 2014. Available online: <https://www.sensefly.com/app/uploads/2017/11/eBee_RTK_Accuracy_Assessment.pdf >. Accessed on 25 Feb 2022